

Coverage Performance of UAV-powered Sensors for Energy-neutral Networks with Recharging Stations

Oktaý Cetinkaya* Mustafa Ozger† David De Roure*

*Oxford e-Research Centre (OeRC)
Department of Engineering Science
University of Oxford, UK
oktay.cetinkaya@eng.ox.ac.uk

†School of Electrical Engineering
and Computer Science
KTH Royal Institute of Technology, Sweden
ozger@kth.se

Abstract—The projected number of Internet of Things (IoT) sensors makes battery maintenance a challenging task. Although battery-less IoT is technologically viable, the sensors should be somehow energized, either locally or remotely. Unmanned aerial vehicles (UAVs) can respond to this quest via wireless power transfer (WPT). However, to achieve energy neutrality across the IoT networks and thus mitigate the maintenance issues, the UAVs providing energy and connectivity to IoT sensors must be supplied by recharging stations having multi-source energy harvesting (EH) capability. Yet, as these sensors rely solely on UAV-transferred power, the absence of UAVs causes sensor outages and hence loss of coverage when they visit recharging stations for battery replenishment. Hence, besides the UAV parameters (e.g., battery size and velocity), recharging duration and station density must be carefully determined to avoid these outages. To address that, this paper uses stochastic geometry to derive the coverage probability of UAV-powered sensors. Our analysis sheds light on the fundamental trade-offs and design guidelines for energy-neutral IoT networks with recharging stations in regard to the regulatory organization limitations, practical rectenna and UAV models, and the minimum power requirements of sensors.

Index Terms—Unmanned Aerial Vehicles, Wireless Power Transfer, Stochastic Geometry, Coverage Probability, IoT.

I. INTRODUCTION

Unmanned aerial vehicles (UAVs) are becoming increasingly essential in wireless networks, serving as either mobile users or base stations/access points (APs) [1]. In addition to the numerous value-added services they already provide, UAVs also play a critical role in addressing the battery constraints of the Internet of Things (IoT) through wireless power transfer (WPT) [2]. They are particularly beneficial for networks that rely on a multitude of sensors, which require excessive maintenance, or that operate in hard-to-reach areas, such as rainforests. By offering line-of-sight (LoS) air-to-ground links, UAVs enable highly efficient WPT [3], which, in turn, enables the battery-less operation of sensors deployed on the ground. After delivering the energy required by sensors, UAVs can also collect sensory data by acting as mobile APs, thereby offering an all-in-one solution. In these settings, UAVs govern both energy and data flows with no human supervision for battery maintenance or terrestrial APs for data collection, aiming for a certain level of autonomy in network operation.

Since the primary goal of a WPT-enabled UAV setting is to minimize the battery constraints of sensors, besides the prevailing energy scarcity across the IoT domain, the energy required for UAV operation, including the power transferred to sensors, has to be provisioned within the network. In this way, *energy neutrality* can be enabled [4], mitigating the challenges mentioned above. One approach for achieving this goal is to replenish UAV batteries via recharging stations having energy harvesting (EH) capability. Here, multiple ambient sources, such as solar and wind power, can be simultaneously exploited [5] to minimize the variance and intermittency in the EH output for assured reliability.

The literature has vast examples of UAV-based service provisioning for IoT devices, including recharging stations. In most cases, the UAVs operate as flying APs [6] to collect sensory data underpinned by terrestrial counterparts. They sometimes deliver power [7] in addition to or aside from AP functionality [8]. The recharging stations are usually deemed to have mains connection, or their source of power is untold [9], both referring to a case with an unlimited energy source, i.e., the total disregard of the energy neutrality objective.

One domain that has been exhaustively studied in the literature is the UAV-assisted IoT networks, in which the UAVs provide coverage to sensors. For example, the authors in [10] optimized the trajectory of a UAV energized by a solar-powered recharging station in consideration of data rate, energy consumption, and fairness of coverage. However, they focused on a single UAV operation without considering the effect of recharging station density, limiting their application potential. Furthermore, the authors in [11] proposed a distributed blockchain-based scheme to enable secure and reliable energy exchange between UAVs and recharging stations. However, they did not consider the energy-neutral operation of their system, leading to an impractical solution. The authors in [12] proposed reinforcement learning algorithms to jointly optimize the velocity and energy replenishment of UAVs that collect data from sensors. Although they enabled efficient transfer learning techniques to decrease the learning time and improve the overall learning process, they did not take energy neutrality into consideration in their setting, similar to other studies.

As discussed in [13] and the references therein, the literature on UAV-assisted sensor coverage mainly focused on various other aspects, such as clustering the sensor nodes for more energy-efficient data collection, different flying modes of UAVs, and joint path planning and resource allocation via graph-theory, optimization, machine learning, etc. Despite the promising findings of these studies, the research must look towards a more pressing and fundamental issue, i.e., how to achieve energy-neutral IoT at the minimal sensor outage, occurring due to recharging station-driven UAV operation. Hence, the following aspects need considerable attention for a more realistic analysis of the coverage performance of sensors, facilitating energy neutrality in the IoT domain: *i*) effective isotropic radiated power (EIRP) limitations enforced by regulatory organizations; *ii*) practical rectenna models with non-linear EH behavior; *iii*) minimum power requirements of sensors; *iv*) individual duration of each UAV operation; and most importantly, *v*) a limited source of power for WPT, i.e., the UAVs energized by multi-source EH recharging stations.

Figure 1: Illustration of the envisioned network scenario.

As illustrated also in Fig. 1, we envision an energy-neutral network scenario, which comprises: *i*) recharging stations, *ii*) UAVs, and *iii*) battery-less sensors. The UAVs retrieve energy from multi-source EH recharging stations via inductive power transfer, fly towards the sensors, energize them via radio frequency (RF) power transfer, and collect their data. During power transfer and data collection, which refers to *service*, the UAVs do not move in the 3D space; they just hover at the centers of event areas, i.e., where sensors reside. The sensors become active as soon as they intercept enough power from a UAV. When active, they probe their vicinity for an application-defined parameter, e.g., temperature, humidity, and/or noise level, and notify their respective UAV with their readings. After collecting sensor data, the UAVs fly back to the nearest recharging station to replenish their batteries.

A. Service Provisioning

In our envisioned scenario, recharging stations refill the UAV battery with energy that is just enough for *i)* a round trip to the event area, i.e., travel to its center and descent/ascent to/from it, *ii)* providing *service*, and *iii)* hovering when providing service. During the trip and getting its battery replenished, the UAV cannot provide any service, i.e., it is unavailable.

The definition above confirms that the service is conditioned on the distance between the point where it is provided and the nearest charging station, $d_\Delta (= R_\Delta + h_l)$. However, only one of d_Δ 's components, namely R_Δ , changes randomly due to the distribution of recharging stations. Hence, the probability of UAV's availability, i.e., the event of service \mathcal{E} , is conditioned on R_Δ , which can be given as:

$$P_{(e|R_\Delta)} = \mathbb{P}(\mathcal{E}|R_\Delta) = \frac{t_{PT} + t_{AP}}{t_{PT} + t_{AP} + t_{Ch} + t_J}, \quad (1)$$

where t_{PT} is the time spent for power transfer, t_{AP} is the time spent for data collection, t_{Ch} is the time spent for recharging the UAV battery, and t_J is the time spent for the round trip. Here, each of t_J , t_{PT} , and t_{AP} can be defined as:

$$\begin{aligned} t_J &= \frac{2(R_\Delta + h_l)}{V} = \frac{2d_\Delta}{V}, \\ t_{PT} &= \frac{E_{PT}}{P_T}, \\ t_{AP} &= \frac{B_{UAV} - t_{PT}(P_h + P_T) - t_J P_J}{P_h}, \end{aligned} \quad (2)$$

where P_J is the power consumption during the trip, V is the UAV's velocity during the trip, E_{PT} is the energy budget spared for power transfer, P_h is the power consumption during hovering at the center of an event area, P_T is the transmit power of the UAV, and B_{UAV} is the energy level of the UAV battery. We should note that the UAV battery might not be fully charged always since it predominately depends on the power transfer rate of the wireless pad, ξ_{Ch} , of the recharging station and the time the UAV spends on it, t_{Ch} . From (1), we also know that t_{Ch} is inversely proportional to UAV availability since it is on the denominator of the equation, so it should be limited. That is also because the UAV battery has a limited/maximum capacity, B_{max} , so the UAV should not reside on the charging pad beyond when the battery gets fully charged, referring to t_{Ch}^{sat} . Note that the saturation time t_{Ch}^{sat} can be achieved sooner or later depending on the charging rate ξ_{Ch} since B_{max} is fixed. Considering all these, an accurate battery charging model for the UAV can be given as:

$$B_{UAV}(t_{Ch}) = \begin{cases} \xi_{Ch} \cdot t_{Ch}, & t_{Ch} \in [0, t_{Ch}^{sat}], \\ B_{max}, & t_{Ch} \geq t_{Ch}^{sat}. \end{cases} \quad (3)$$

and finally, by taking the expectation of (1), the service probability of the UAV can be calculated as:

$$P_e = \mathbb{E}_{\Phi_{Ch}} \left[\frac{t_{PT} + t_{AP}}{t_{PT} + t_{AP} + t_{Ch} + t_J} \right]. \quad (4)$$

B. Power Transfer

The UAV performs RF power transfer with a directional antenna having a pencil-beam-like radiation pattern. For such an antenna, i.e. with one major lobe and very negligible minor

lobes of the beam, the gain G_T can be approximated by:

$$G_T = \begin{cases} \approx \frac{30000}{\theta_B^2}, & \frac{-\theta_B}{2} \leq \varphi \leq \frac{\theta_B}{2}, \quad (\text{major lobe}) \\ g(\varphi), & \text{otherwise,} \quad (\text{minor lobes}) \end{cases} \quad (5)$$

where φ is the sector angle, θ_B is the directional antenna half-power beamwidth (HPBW) -both in degrees, $\approx 30000/\theta_B^2$ is the maximum gain, and $g(\varphi)$ is the gain outside of the major lobe (including minor lobes), which can be neglected [14]. Note that (5) is for a symmetrical radiation pattern, where the HPBWs in each plane are equal to each other, i.e. $\theta_{1d} = \theta_{2d}$.

Contrary to expectations, the transmit power of the UAV, P_T in (2), cannot be altered casually; it is determined by regulatory organizations, e.g., the Office of Communications (Ofcom) in the UK, the Federal Communications Commission (FCC) in the US. For example, FCC Part 15.247 rules [15] declare that the maximum P_T fed into the (in our case, UAV's) antenna cannot exceed 30dBm (1W) for the industrial, scientific, and medical (ISM) bands, in which the maximum effective isotropic radiated power (EIRP_{max}) is limited to 36dBm (4W). This indicates that increasing G_T necessitates a proportional decrease in P_T , and vice versa, such that the total RF power radiated by the antenna remains the same, i.e., 4W EIRP, where $\max(P_T) = 1W$ for each case. For directional dispersion, however, there are some exceptions to the EIRP_{max}, details of which can be found in [15].

Here, we should note the following: *i)* since the antenna size increases with increasing G_T , the G_T vs. P_T balance must be maintained regarding what a UAV can physically accommodate, *ii)* power transfer should be administrated at a low frequency (f , preferably sub-GHz), as the power received by sensors (P_R) is inversely proportional to the square of f , i.e., $P_R \propto 1/f^2$, *iii)* since the UAV has a fixed budget for power transfer (E_{PT}), decreasing P_T means a longer t_{PT} , which may affect the service probability of the UAV -from (1). The lengthened coverage lifetime, t_{PT} , despite sounding attractive, will alter the duty cycle of sensors, which cannot be tolerated always due to the certain reporting frequency requirements of IoT applications [16]. Thus, these trade-offs must be carefully considered during the system design to maximize the performance metric defined by the application.

C. Trip Power Consumption

The rotary-wing type UAVs that we have need fixed power during their trip, which can be approximated as [17]:

$$P_J(V) \approx P_0 \left(1 + \frac{3V^2}{U_{tip}^2} \right) + \frac{P_i v_0}{V} + \frac{1}{2} d_0 \rho s A V^3, \quad (6)$$

where U_{tip}^2 is the tip speed of the rotor blade, v_0 is the mean rotor-induced velocity when hovering, d_0 is the fuselage drag ratio, ρ is the air density, s is the rotor solidity, A is the rotor disc area, and P_0 and P_i are the UAV's blade profile power and induced power in hovering status, respectively. Here, P_h

can be defined as the sum of P_0 and P_i , i.e.,:

$$P_h = \underbrace{\frac{\delta}{8} \rho s A \Omega^3 R^3}_{\triangleq P_0} + \underbrace{(1+k) \frac{W^{3/2}}{\sqrt{2\rho A}}}_{\triangleq P_i}, \quad (7)$$

where Ω is the blade angular velocity, R is the rotor radius, k is the incremental correction factor to induced power, and W is the UAV weight. Using the respective values of each parameter given in [17], P_J as a function of V is illustrated in Fig. 2(a), which is also used in our calculations.

From (2) and (6), the energy that the UAV needs for a round trip, E_J , is $t_J \times P_J = \frac{2(R_{\Delta} + h_i)}{V} P_J$, where each leg consumes the half, i.e., $E_J/2$ for travelling to or from the service point. That is important, as the energy left in B_{UAV} after providing service must be enough for UAV to make it to the nearest charging station before depleting its battery, i.e., $E_{\text{left}} \geq E_J/2$. In our analyses, we evaluate the effect of V in minimizing E_J , ensuring that the UAV has more resources for *service*.

D. Sensor Association

We assume that each event area, Δ , is serviced by only one UAV at a time, i.e., each sensor is associated with one UAV hovering at the center of Δ that the sensor falls into. Otherwise, the sensor has no service, which refers to the outage.

The power intercepted by the sensor, P_I , after the UAV initializes the power transfer process is:

$$P_{I_\chi} = \frac{\text{EIRP}^+ G_R G_h}{\text{PL}_\chi}, \quad (8)$$

where EIRP^+ is equal to $P_T \times G_T$, G_R is the gain of sensor antenna, G_h is exponentially distributed fading power coefficient, PL is path loss as a function of distance between the UAV and sensor, and finally, χ refers to LoS and NLoS, i.e., the line of sight (LoS) and Non-LoS, indicating the condition of the air-to-ground link between the UAV and sensors.

To perform sensory operations, however, P_{I_χ} has to be converted into utilizable DC power, P_{R_χ} , using a rectifying antenna or *rectenna*. Considering the sensitivity and saturation of rectennas, the research field has agreed on the following

piecewise linear function, capturing P_{R_χ} as a high-order polynomial [19]:

$$P_{R_\chi}(P_{I_\chi}) \triangleq \begin{cases} 0, & P_{I_\chi} \in [0, P_{th}), \\ (p_w + \sum_{j=1}^{w-1} p_j P_{I_\chi}^{w-j}) \cdot P_{I_\chi}, & P_{I_\chi} \in [P_{th}, P_{sat}], \\ P_{R_\chi}(P_{sat}), & P_{I_\chi} \geq P_{sat}, \end{cases} \quad (9)$$

where $P_{R_\chi}(P_{I_\chi})$ is non-decreasing and continuous for all $P_{I_\chi} \in \mathbb{R}$, $P_{I_\chi} \geq 0$. In our analyses, the rectennas are assumed to operate in the ideal region, i.e., $P_{I_\chi} \in [P_{th}, P_{sat}]$ for all sensors. Hence, $(p_w + \sum_{j=1}^{w-1} p_j P_{I_\chi}^{w-j})$ is the rectenna (or RF-to-DC conversion) efficiency as a function of P_{I_χ} , i.e., $\Psi(P_{I_\chi})$ ($0 \leq \Psi(P_{I_\chi}) < 1$), with w being the degree of polynomial and $\{p_j\}_{j=1}^w$ the respective coefficients. Furthermore, $\Psi(P_{I_\chi})$ is calculated using real data outsourced from [18], where Fig. 2(b) depicts the measured and simulated behaviors of the rectenna design of authors.

PL_{LoS} and PL_{NLoS} in (8) can be given as [20]:

$$\begin{aligned} \text{PL}_{\text{LoS}} &= 20 \log_{10} \left(\frac{4\pi f_c d_{3D}}{c} \right) + \eta_{\text{LoS}}, \\ \text{PL}_{\text{NLoS}} &= 20 \log_{10} \left(\frac{4\pi f_c d_{3D}}{c} \right) + \eta_{\text{NLoS}}, \end{aligned} \quad (10)$$

where f_c is the carrier frequency, c is the speed of light, and η_{LoS} , η_{NLoS} are average additional loss, depending on the environment for LoS, and NLoS links, respectively. Furthermore, the probability that the UAV has a LoS air-to-ground link with a sensor can be formulated as [21]:

$$P_{\text{LoS}} = \frac{1}{1 + \gamma \exp(-\delta(90 - \theta_B/2 - \gamma))}, \quad (11)$$

where γ and δ are constant values that depend on the environment (e.g., suburban, high-rise urban), and $(90 - \theta_B/2)$ is the elevation angle of the UAV. Finally, the probability of NLoS is always $P_{\text{LoS}} = 1 - P_{\text{NLoS}}$.

Based on the equations given above, we can define the coverage probability of the UAV conditioned on R_{Δ} as:

$$P_{\text{cov}|R_{\Delta}} = P_{(e|R_{\Delta})} P_{\text{cov},s}, \quad (12)$$

where $P_{(e|R_{\Delta})}$ is given in (1). Hence, the unconditional coverage probability can be expressed as:

$$P_{\text{cov}} = P_e P_{\text{cov},s}, \quad (13)$$

in which:

$$P_{\text{cov},s} = \mathbb{P}(P_{R_\chi} \geq \Gamma_{th}), \quad (14)$$

where Γ_{th} is the minimum power that has to be received by a sensor to become active, referring to the sensitivity, probe its vicinity, and deliver the data it collects to the UAV. Here, we should note that d_{3D} , and so R_{RF} , can be assumed as equal to h_{UT} due to directivity ($h_{UT} = \cos(\theta/2) \times R_{RF}$ actually, but $\theta/2$ is quite small; hence, $R_{RF} \approx h_{UT}$). That leads to the assumption that P_{R_χ} will be equal for each point in the

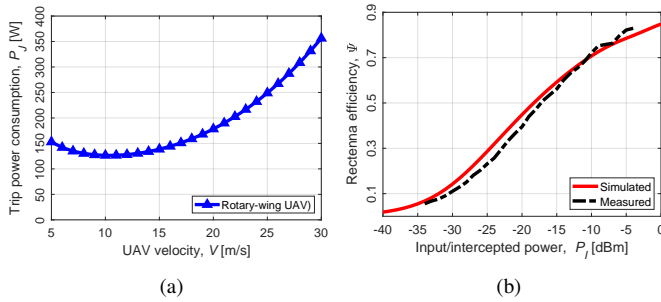


Figure 2: (a) Trip power consumption, P_J , vs. UAV velocity, V , as modelled in [17]; (b) rectenna efficiency, Ψ , as a function of input/intercepted power, P_{I_χ} , for the rectenna in [18] ($@f_c = 868\text{MHz}$).

event area, i.e., all sensors in Δ will receive the same power irrespective of their locations. Therefore, P_{R_x} does not need to be averaged when $P_{\text{cov},s}$ is calculated.

III. PERFORMANCE METRICS

In this section, we first derive the service probability conditioned on the distance to the nearest charging station, i.e., $P_{(e|R_\Delta)}$, to calculate the unconditioned service probability, P_e . Then, we find $P_{\text{cov},s}$, and hence, study the coverage probability, P_{cov} , for the envisioned energy-neutral network scenario.

A. Service Probability

By substituting for (2) in (1), we can derive the service probability given the value of R_Δ as:

$$P_{(e|R_\Delta)} = \frac{\zeta - 2(R_\Delta + h_l)P_J}{\zeta - 2(R_\Delta + h_l)(P_J - P_h) + Vt_{Ch}P_h}, \quad (15)$$

where $\zeta = VB_{UAV} - Vt_{PT}P_T$. It should be noted that (15) only holds if $R_\Delta \leq \frac{VB_{UAV} - 2h_lP_J}{2P_J}$; otherwise, $P_{(e|R_\Delta)} = 0$. If this condition is not satisfied, it means that B_{UAV} is not large enough to support the energy required for the round trip. Hence, there will not be enough power for the UAV to provide service in Δ . In addition, when $R_\Delta = 0$, h_l is also 0, because the UAV cannot descent when it is still on the recharging station. In that case, the maximum service probability is achieved, i.e., $P_{(e|R_\Delta=0)} = \frac{\zeta}{\zeta + Vt_{Ch}P_h}$.

Now, using (15), let's calculate the CDF of the conditional service probability, $F_{P_{(e|R_\Delta)}}(x)$, as:

$$\begin{aligned} F_{P_{(e|R_\Delta)}}(x) &= \mathbb{P}(P_{(e|R_\Delta)} \leq x) \\ &= \mathbb{P}\left(\frac{\zeta - 2(R_\Delta + h_l)P_J}{\zeta - 2(R_\Delta + h_l)(P_J - P_h) + Vt_{Ch}P_h} \leq x\right), \end{aligned}$$

and given that $P_{(e|R_\Delta)}$ is a decreasing function of R_Δ , the preimage can be obtained as:

$$= \mathbb{P}\left(R_\Delta \geq \frac{\zeta(1-x) - h_l\kappa - xVt_{Ch}P_h}{\kappa}\right), \quad (16)$$

where $\kappa = 2[P_J(1-x) + xP_h]$.

Hence, the CDF becomes:

$$F_{P_{(e|R_\Delta)}}(x) = e^{-\lambda_{Ch}\pi Q^2(x)}, \quad (17)$$

in which:

$$Q(x) = \frac{\zeta(1-x) - h_l\kappa - xVt_{Ch}P_h}{\kappa}.$$

Since the minimum value of $R_\Delta = 0$, and its maximum value for a non-zero availability probability is $\frac{VB_{UAV} - 2h_lP_J}{2P_J}$, then:

$$0 \leq x \leq \frac{\zeta}{\zeta + Vt_{Ch}P_h}$$

Using these results, we can find the service probability as:

$$\begin{aligned} P_e &= \mathbb{E}_{\Phi_{Ch}}[P_{(e|d_\Delta)}] \\ &= \int_0^\infty (1 - F_{P_{(e|d_\Delta)}}(x)) dx \\ &= \int_0^{\frac{\zeta}{\zeta + Vt_{Ch}P_h}} (1 - e^{-\lambda_{Ch}\pi Q^2(x)}) dx. \end{aligned} \quad (18)$$

B. Coverage Probability

Based on the equations derived in the previous subsections, we can now work on the coverage probability given in (14). First, we need to reexpress $P_{\text{cov},s}$ as follows:

$$\begin{aligned} P_{\text{cov},s} &= P_{\text{covLoS}}P_{\text{LoS}} + P_{\text{covNLoS}}P_{\text{NLoS}} \\ &= \mathbb{P}(P_{R_{\text{LoS}}} \geq \Gamma_{th})P_{\text{LoS}} + \mathbb{P}(P_{R_{\text{NLoS}}} \geq \Gamma_{th})P_{\text{NLoS}} \\ &= \mathbb{P}(\eta_{\text{LoS}} \frac{\text{EIRP}^+_{RG_RG_h}}{\text{PL}_{\text{LoS}}} \geq \Gamma_{th})P_{\text{LoS}} + \dots \\ &\quad \dots + \mathbb{P}(\eta_{\text{NLoS}} \frac{\text{EIRP}^+_{RG_RG_h}}{\text{PL}_{\text{NLoS}}} \geq \Gamma_{th})P_{\text{NLoS}} \\ &= \mathbb{P}\left(G_h \geq \frac{\Gamma_{th}\text{PL}_{\text{LoS}}}{\eta_{\text{LoS}}\text{EIRP}^+_{RG_R}}\right)P_{\text{LoS}} + \mathbb{P}\left(G_h \geq \frac{\Gamma_{th}\text{PL}_{\text{NLoS}}}{\eta_{\text{NLoS}}\text{EIRP}^+_{RG_R}}\right)P_{\text{NLoS}} \\ &= e^{-\left(\frac{\Gamma_{th}\text{PL}_{\text{LoS}}}{\eta_{\text{LoS}}\text{EIRP}^+_{RG_R}}\right)}P_{\text{LoS}} + e^{-\left(\frac{\Gamma_{th}\text{PL}_{\text{NLoS}}}{\eta_{\text{NLoS}}\text{EIRP}^+_{RG_R}}\right)}P_{\text{NLoS}}. \end{aligned} \quad (19)$$

Therefore, the coverage probability, P_{cov} in (13), can be finally calculated by using (18) and (19).

IV. NUMERICAL RESULTS

In this section, we calculate the coverage probability using the derived equations to study the effect of recharging time and station density, maximum battery size, and UAV speed. Unless otherwise stated, Table I provides the parameter values, where η_{LoS} and η_{NLoS} are for high-rise urban scenario.

We first investigate the effect of varying recharging time on the coverage probability for an increasing recharging station density. For this analysis, using (3) for the considered B_{max} and ξ_{Ch} values, we know that t_{Ch}^{sat} should be 3600 seconds, i.e., 1 hour, which is typical for commercial UAVs. Fig. 3(a) depicts

Table I: Parameter values.

Service-related			
P_T	21 [dBm]	G_T	15 [dBi]
θ_B	30.8 [°]	f_c	868 [MHz]
c	3×10^8 [m/s]	Γ_{th}	1 [μ W]
Environment-related		[22]	
η_{LoS}	1.6034 [dB]	γ	27.1157
η_{NLoS}	29.6462 [dB]	δ	0.1232
UAV-related		[17]	
B_{max}	770 [Wh]	P_h	168.48 [W]
V	10.36 [m/s]	P_J	126.395 [W]
Others			
λ_{Ch}	10^{-6} [m ⁻²]	G_R	9 [dBi]
h_{Ch}	100 [m]	h_l	80 [m]

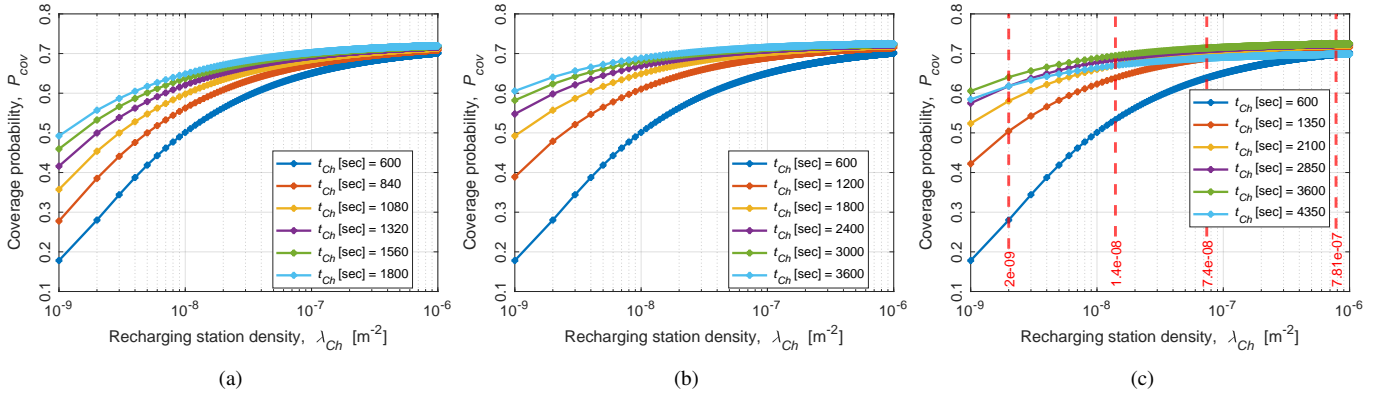


Figure 3: Coverage probability, P_{cov} , vs. recharging station density, λ_{Ch} , for different t_{Ch} : (a) half-charged; (b) fully-charged; (c) overflowed.

what happens when the UAV stays at the recharging station until its battery gets half-full gradually. Here, we observe that, depending on the recharging level, certain discrepancies arise, which are especially evident for lower densities of recharging stations. For example, in the case of 0.001 stations per km², P_{cov} gets 2.7 times better when t_{Ch} is increased from 600 to 1800 seconds. This effect is less apparent for higher λ_{Ch} because finding a recharging station becomes more likely for the UAV; hence, it may not need to depend heavily on the charge in its battery due to the increased recharging possibility. Numerically speaking, P_{cov} increases only up to 1.3 times for the same increment in t_{Ch} when λ_{Ch} is ten times higher, i.e., 0.01 per km². When we look at the fully charged case shown in Fig.3(b), which can be considered ideal in theory, we see that the performance gap increases for lower-density values. Unsurprisingly, a fully-charged battery can help the UAV achieve better coverage, especially at a low λ_{Ch} , compared to those of partially-charged cases. Finally, in Fig.3(c), we analyze the case when the battery overflowed, i.e., when the UAV continues to stay at the recharging station after its battery gets fully charged. From (1), we know that increasing t_{Ch} beyond saturation is unsuggested since the service probability, P_e , and hence P_{cov} , is inversely proportional to it. However, Fig.3(c) reveals that this might not be the case always. As seen, when the battery is charged for 4350 seconds ($> t_{Ch}^{sat}$), it is still possible to obtain higher P_{cov} compared to the partial charge cases, depending on λ_{Ch} . For example, t_{Ch} of 600 seconds can only outperform the overflowed case when λ_{Ch} is $7.81 \times 10^{-6} \text{m}^{-2}$ or higher. Similar comments also hold for other t_{Ch} values (except for t_{Ch}^{sat}), as can be seen from the dashed red lines perpendicular to the x-axis, where the λ_{Ch} threshold significantly reduces for increasing charge level towards the full battery, e.g., $2 \times 10^{-9} \text{m}^{-2}$ for t_{Ch} of 2850 seconds. The take-home message from this analysis is that a relatively empty battery might be worse than overstaying at the recharging station, e.g., for maintenance purposes, if the application mandates a certain level of λ_{Ch} .

Next, we extend our discussion to the impact of using batteries of different sizes on the coverage probability for varying charging times. As can be seen from Fig. 4(a), in

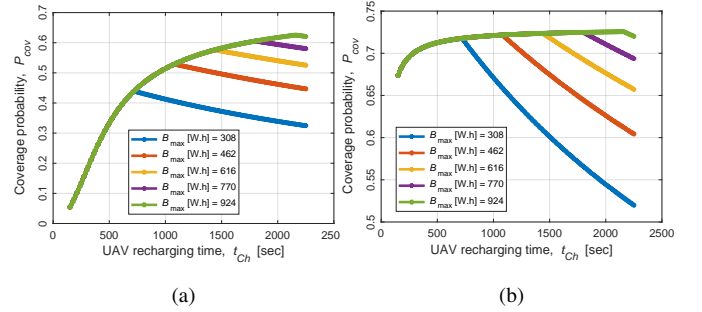


Figure 4: Coverage probability, P_{cov} , vs. recharging time, t_{Ch} , for different B_{max} : (a) @ $\lambda_{Ch} = 10^{-9} \text{m}^{-2}$; (b) @ $\lambda_{Ch} = 10^{-6} \text{m}^{-2}$.

the case of a partial charge, all batteries show the same performance until $t_{Ch} = 1440$ seconds, i.e., when the battery of size 308Wh gets full. That is because all batteries are charged to the same level at that t_{Ch} value regardless of their total size, B_{max} . The same phenomenon is also observed for the remaining batteries until the one with the smallest size reaches its t_{Ch}^{sat} , where the respective P_{cov} starts its dramatic decay due to overflow. Fig. 4(a) and Fig. 4(b) are for different densities of stations; 10^{-9} and 10^{-6}m^{-2} , respectively. Although t_{Ch}^{sat} of each battery remains the same, the achievable P_{cov} changes dramatically due to the clockwise rotation of the behavior.

We lastly focus on understanding how the UAV velocity affects the coverage performance depending on the recharging station density. Before explaining the results, we should note that Fig. 5 is produced for a B_{max} of 192.5Wh, i.e., the quarter of what Table I mentions, which is only charged until its half at the same rate. As seen, the impact of V is negligible for high λ_{Ch} due to the same reason explained earlier in this section. For low λ_{Ch} , on the other hand, the UAV should speed up to reach the nearest station faster, although that means an increased P_J . Due to the P_J component, however, the increment in V is only beneficial until a certain point, as shown with the black dashed line marking the optimal velocity values for each λ_{Ch} . Using a bigger battery and charging it to the ideal level, i.e., 100% -no overflow, will diminish this behavior, forcing higher speeds only for low λ_{Ch} values.

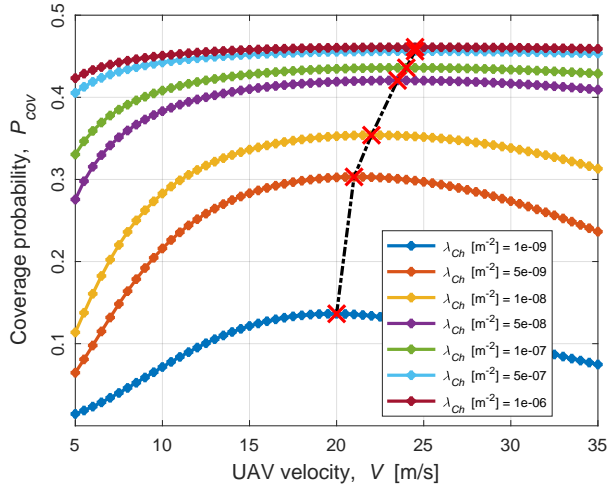


Figure 5: Coverage probability, P_{cov} , as a function of UAV velocity, V , for varying λ_{Ch} values.

The results above suggest that for a given performance target, e.g., maximum P_{cov} with minimum λ_{Ch} , shorter t_{Ch} , or a fixed B_{max} , the relevant design parameters can be tweaked as required. Considering that most of these parameters affect each other, e.g., the EIRP limit on P_T alters not only P_{LoS} (due to the dictated θ_B) but also the size of the event area and hence the number of sensors that can be powered (not within the scope of this study) and even their reporting frequencies, the network requires a holistic design approach as optimizing the trade-offs for the best performance achievable. We believe this paper provides a practice-based showcase on this, providing guidance for future efforts.

V. CONCLUSIONS

This study investigates the factors affecting the coverage performance of sensors energized by UAVs with directional antennae, constituting an energy-neutral IoT network together with the multi-source EH recharging stations replenishing UAVs batteries. With this goal, We first derived the service probability as a function of UAV power consumption/velocity and battery size, recharging time and station density, and WPT duration. That was then joined with distance-conditioned coverage probability, incorporating the effects of directivity, the LoS/NLoS connectivity, and the non-linear EH model. The analyses revealed the design considerations for the best coverage with regard to FCC regulations, realistic rectenna and UAV operation, and minimum power requirements of sensors. Future works will focus on calculating the number of sensors that can be powered by UAVs. We will also try maximizing the communication throughput of sensors in the envisioned setting by optimizing the parameters/trade-offs that have been discussed in this study.

VI. ACKNOWLEDGEMENT

This work has been supported by the PETRAS National Centre of Excellence for IoT Systems Cybersecurity, funded by the UK EPSRC under grant number EP/S035362/1.

REFERENCES

- [1] A. Baltaci *et al.*, "A Survey of Wireless Networks for Future Aerial Communications (FACOM)," *IEEE Communications Surveys & Tutorials*, vol. 23, no. 4, pp. 2833–2884, 2021.
- [2] O. Cetinkaya and G. V. Merrett, "Efficient Deployment of UAV-powered Sensors for Optimal Coverage and Connectivity," in *IEEE Wireless Communications and Networking Conference (WCNC)*, 2020, pp. 1–6.
- [3] X. Yuan *et al.*, "Joint Design of UAV Trajectory and Directional Antenna Orientation in UAV-enabled Wireless Power Transfer Networks," *IEEE Journal on Selected Areas in Communications*, vol. 39, no. 10, pp. 3081–3096, 2021.
- [4] T. Long *et al.*, "Energy Neutral Internet of Drones," *IEEE Communications Magazine*, vol. 56, no. 1, pp. 22–28, 2018.
- [5] O. B. Akan *et al.*, "Internet of Hybrid Energy Harvesting Things," *IEEE Internet of Things Journal*, vol. 5, no. 2, pp. 736–746, 2018.
- [6] M. Alzenad *et al.*, "3-D Placement of an Unmanned Aerial Vehicle Base Station (UAV-BS) for Energy-efficient Maximal Coverage," *IEEE Wireless Communications Letters*, vol. 6, no. 4, pp. 434–437, 2017.
- [7] L. Xie *et al.*, "UAV-enabled Wireless Power Transfer: A Tutorial Overview," *IEEE Transactions on Green Communications and Networking*, vol. 5, no. 4, pp. 2042–2064, 2021.
- [8] H.-T. Ye *et al.*, "Optimization for Wireless-powered IoT Networks enabled by an Energy-limited UAV Under Practical Energy Consumption Model," *IEEE Wireless Communications Letters*, vol. 10, no. 3, pp. 567–571, 2020.
- [9] Y. Qin *et al.*, "Performance Evaluation of UAV-enabled Cellular Networks with Battery-limited Drones," *IEEE Communications Letters*, vol. 24, no. 12, pp. 2664–2668, 2020.
- [10] L. Zhang *et al.*, "Energy-Efficient Trajectory Optimization for UAV-Assisted IoT Networks," *IEEE Transactions on Mobile Computing*, vol. 21, no. 12, pp. 4323–4337, 2022.
- [11] V. Hassija *et al.*, "A Distributed Framework for Energy Trading Between UAVs and Charging Stations for Critical Applications," *IEEE Transactions on Vehicular Technology*, vol. 69, no. 5, pp. 5391–5402, 2020.
- [12] N. H. Chu *et al.*, "Joint Speed Control and Energy Replenishment Optimization for UAV-assisted IoT Data Collection with Deep Reinforcement Transfer Learning," *IEEE Internet of Things Journal*, pp. 1–1, 2022.
- [13] Z. Wei *et al.*, "UAV-assisted Data Collection for Internet of Things: A Survey," *IEEE Internet of Things Journal*, vol. 9, no. 17, pp. 15 460–15 483, 2022.
- [14] C. A. Balanis, *Antenna Theory: Analysis and Design*. John Wiley & sons, 2015.
- [15] "Federal Communications Commission CFR, Title 47, Volume 1, Part 15," <https://www.govinfo.gov/app/details/CFR-2010-title47-vol1>, 2010.
- [16] O. Cetinkaya and O. B. Akan, "Electric-Field Energy Harvesting From Lighting Elements for Battery-Less Internet of Things," *IEEE Access*, vol. 5, pp. 7423–7434, 2017.
- [17] Y. Zeng *et al.*, "Energy Minimization for Wireless Communication with Rotary-wing UAV," *IEEE Transactions on Wireless Communications*, vol. 18, no. 4, pp. 2329–2345, 2019.
- [18] M. Wagih *et al.*, "High-efficiency sub-1 GHz Flexible Compact Rectenna based on Parametric Antenna-rectifier Co-design," in *2020 IEEE/MTT-S International Microwave Symposium (IMS)*, 2020, pp. 1066–1069.
- [19] P. N. Alevizos *et al.*, "Nonlinear Energy Harvesting Models in Wireless Information and Power Transfer," in *2018 IEEE 19th International Workshop on Signal Processing Advances in Wireless Communications (SPAWC)*. IEEE, 2018, pp. 1–5.
- [20] J. Li *et al.*, "Joint Optimization on Trajectory, Altitude, Velocity, and Link Scheduling for Minimum Mission Time in UAV-aided Data Collection," *IEEE Internet of Things Journal*, vol. 7, no. 2, pp. 1464–1475, 2019.
- [21] Z. Liao *et al.*, "HOTSPOT: A UAV-assisted Dynamic Mobility-aware Offloading for Mobile-edge Computing in 3-D Space," *IEEE Internet of Things Journal*, vol. 8, no. 13, pp. 10940–10952, 2021.
- [22] A. Almarhabi *et al.*, "LoRa and High-altitude Platforms: Path Loss, Link Budget and Optimum Altitude," in *2020 8th International Conference on Intelligent and Advanced Systems (ICIAS)*. IEEE, 2021, pp. 1–6.